

Nearest Neighborhood-Based Deep Clustering for Source Data-absent Unsupervised Domain Adaptation

Song Tang, *Member, IEEE*, Yan Yang, Zhiyuan Ma, *Member, IEEE*, Norman Hendrich, Fanyu Zeng, *Member, IEEE*, Shuzhi Sam Ge, *Fellow, IEEE*, Changshui Zhang, *Fellow, IEEE*, and Jianwei Zhang, *Member, IEEE*

Abstract—In the classic setting of unsupervised domain adaptation (UDA), the labeled source data are available in the training phase. However, in many real-world scenarios, owing to some reasons such as privacy protection and information security, the source data is inaccessible, and only a model trained on the source domain is available. This paper proposes a novel deep clustering method for this challenging task. Aiming at the dynamical clustering at feature-level, we introduce extra constraints hidden in the geometric structure between data to assist the process. Concretely, we propose a geometry-based constraint, named semantic consistency on the nearest neighborhood (SCNNH), and use it to encourage robust clustering. To reach this goal, we construct the nearest neighborhood for every target data and take it as the fundamental clustering unit by building our objective on the geometry. Also, we develop a more SCNNH-compliant structure with an additional semantic credibility constraint, named semantic hyper-nearest neighborhood (SHNNH). After that, we extend our method to this new geometry. Extensive experiments on three challenging UDA datasets indicate that our

method achieves state-of-the-art results. The proposed method has significant improvement on all datasets (as we adopt SHNNH, the average accuracy increases by over 3.0% on the large-scaled dataset). Code is available at <https://github.com/tntek/N2DCX>.

Index Terms—Nearest neighborhood, Deep clustering, Semantic consistency, Classification, Unsupervised domain adaptation.

I. INTRODUCTION

BEING a branch of transfer learning [1], unsupervised domain adaptation (UDA) [2] intends to perform an accurate classification on the unlabeled test set given a labeled train set. In UDA, we specialize the train and test sets with different probability distributions as the source domain and target domain, respectively. During the transfer (training) process, we assume the labeled source data is to be accessible in the problem setting of UDA.

The key to solving UDA is to reduce the domain drift. Because of data available from both domains, the existing methods mainly convert UDA to probability distribution matching problems, i.e., domain alignment, where the domain data represent the corresponding domain's probability distribution. However, access to the source data is becoming extremely difficult. First, as the evolution of algorithms begins to wane, the performance improvements primarily rely on the increase of large-scale labeled data with high quality. It is hard to obtain data, deemed as a vital asset, at a low cost. Companies or organizations may release learned models but cannot provide their customer data due to data privacy and security regulations. Second, in many application scenarios, the source datasets (e.g., videos or high-resolution images) are becoming very large. It will often be impractical to transfer or retrain them to different platforms.

Therefore, the so-called *source data-absent UDA (SAUDA)* problem considers the scenario where only a source model pre-trained on the source domain and the unlabeled target data are available for the transfer (training) phase. Namely, we can only use the source data for the source model training. As most UDA methods cannot support this tough task due to their dependence on source data to perform distribution matching, this challenging topic has recently attracted a lot of research [3], [4], [5], [6], [7].

Due to its independence from given supervision information, self-supervised learning becomes a central concept for

This work has been submitted to the IEEE for possible publication. Copyright may be transferred without notice, after which this version may no longer be accessible.

This work is partly funded by the German Research Foundation and the National Natural Science Foundation of China in the Crossmodal Learning project under contract Sonderforschungsbereich Transregio 169, the Hamburg Landesforschungsförderungsprojekt Cross, the National Natural Science Foundation of China (61773083); Horizon2020 RISE project STEP2DYNA (691154); the National Key R&D Program of China (2018YFE0203900, 2020YFB1313600); the National Natural Science Foundation of China (U1813202, 61773093); the Shanghai Artificial Intelligence Innovation Development Special Support Project, R & D and Industrialization (3920365001); the Sichuan Science and Technology Program (2020YFG0476); Open Project of State Key Lab. for Novel Software Technology, Nanjing University, Nanjing, China (KFKT2021B39). (*Corresponding authors: Jianwei Zhang.*)

Song Tang are with the Institute of Machine Intelligence, University of Shanghai for Science and Technology, Shanghai, China; the State Key Laboratory of Electronic Thin Films and Integrated Devices, University of Electronic Science and Technology of China, Chengdu, China; the Technical Aspects of Multimodal Systems (TAMS) Group, Department of Informatics, Universität Hamburg, Hamburg, Germany. (e-mail: tntechlab@hotmail.com)

Yan Yang are with the Institute of Machine Intelligence, University of Shanghai for Science and Technology, Shanghai, China

Zhiyuan Ma are with the Institute of Machine Intelligence, University of Shanghai for Science and Technology, Shanghai, China; the State Key Lab. for Novel Software Technology, Nanjing University, Nanjing, China.

Fanyu Zeng is with the Engineering Research Center of Wideband Wireless Communication Technology, Ministry of Education, Nanjing University of Posts and Telecommunications, Nanjing, China.

Shuzhi Sam Ge is with the Department of Electrical and Computer Engineering, National University of Singapore, Singapore.

Changshui Zhang is with the Department of Automation, Tsinghua University, Beijing, China.

Norman Hendrich and Jianwei Zhang are with the Technical Aspects of Multimodal Systems (TAMS) Group, Department of Informatics, Universität Hamburg, Hamburg, Germany.

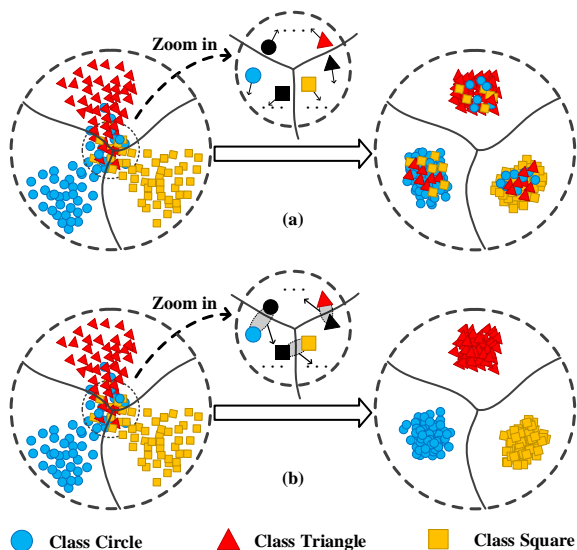


Fig. 1: Illustration of the NNH-based deep clustering. (a) and (b) present a deep clustering taking individual data and the nearest neighborhood (NNH) of single data as fundamental clustering units, respectively.

solving unsupervised learning problems. As an important self-supervised scheme, deep clustering has made progress in many unsupervised scenarios. For example, [8] developed an end-to-end general method with pseudo-labels from self-labelling for unsupervised learning of visual features. Very recently, [5] extended the work proposed in [8] to SAUDA, following the hypothesis transfer framework [9]. Essentially, these methods equivalently implement a deep clustering built on individual data, as shown in Fig. 1(a). Although achieving excellent results, this individual-based clustering process is susceptible to external factors, such as pseudo-label errors. As a result, some samples move towards a wrong cluster (see the middle and the right subfigure in Fig. 1(a)).

Holding the perspective of robust clustering, in this paper, we intend to mine a correlation (constraint) from the local geometry of data for more robust clustering. If we take the nearest neighborhood (NNH) of individual data as the fundamental unit, the clustering may group more robustly. As shown in the middle subfigure of Fig. 1(b), the black circle (misclassified sample) moves to the wrong cluster. However, the gray oval (the nearest neighborhood) may move to the correct cluster with the help of an adjustment from the blue circle (the nearest neighbor that is correctly classified). Maintaining this trend, the gray oval, including the black circle (misclassified sample), can eventually cross the classification plane and reach the correct cluster.

Inspired by the idea above, this paper proposes a new deep clustering-based SAUDA method. The key of our method is to encourage NNH geometry, i.e., the gray oval in Fig. 1(b), to move correctly instead of moving the individual data. We achieve this goal in two ways. Firstly, we propose a new constraint on the local geometry, named semantic consistency on nearest neighborhood (SCNNH). A law of cognition inspires it: the most similar objects are likely to belong to

the same category, discovered by research on infant self-learning [10]. Secondly, based on the backbone in [8], [5], we propose a novel framework to implement the clustering on NNH. Specifically, besides integrating a geometry constructor to build NNH for all data, we generate the pseudo-labels based on a semantic fusion on NNH. Also, we give a new SCNNH-based regularization to regulate the self-training.

Moreover, we give an advanced version of our method. This method proposes a new, more SCNNH-compliant implementation of NNH, named semantic hyper-nearest neighborhood (SHNNH), and extends the proposed adaptation framework to this geometry. The contributions of this paper cover the following three areas.

- We exploit a new way to solve SAUDA. We introduce the semantic constraint hidden in the local geometry of individual data, i.e., NNH, to encourage robust clustering on the target domain. Correspondingly, we propose a new semantic constraint upon NNH, i.e., SCNNH.
- Based on the SCNNH constraint, we propose a new deep clustering-based adaptation method building on NNH instead of individual data. Moreover, we extend our method to a newly designed geometry, i.e., SHNNH, which expresses SCNNH more reasonably. Different from the construction strategy only based on spatial information, we additionally introduce semantic credibility constraints in the new structure.
- We perform extensive experiments on three challenging datasets. The results of the experiment indicate that our approach achieves state-of-the-art performance on both developed geometries. Also, except for the ablation study to explore the effect of the components in our method, a careful investigation is conducted in the analysis part.

The remainder of this paper is organized as follows. Section II introduces the related work, followed by the preliminary work as Section III. Section IV details the proposed method, while Section V extends our approach to a semantic credibility-based NNH. Section VI gives the experimental results and related analyses. In the end, we present the conclusion in Section VII.

II. RELATED WORK

A. Unsupervised Domain Adaptation

At present, UDA methods are widely used in scenarios such as medical image diagnosis [11], semantic segmentation [12], and person re-identification [13]. The existing methods mainly rely on probability matching to reduce the domain drift, i.e., diminishing the probability distributions' discrepancies between the source and target domains. Based on whether to use deep learning algorithms, current methods can be divided into two categories. In the first category (i.e., deep learning-based methods), researchers rely on techniques such as metric learning to reduce the domain drift [14], [15], [16]. In these methods, an embedding space with unified probability distribution is learned by minimizing certain statistical measures (e.g., maximum mean discrepancy), which are used to evaluate the discrepancy of the domains. Also, adversarial learning has been another popular framework due

to its capability of aligning the probabilities of two different distributions [17], [18], [19]. As for the second class, the non-deep-learning methods reduce the drift in diverse manners. From the aspect of geometrical structure, [20], [21], [22] model the transfer process from the source domain to the target one based on the manifold of data. [23] perform the transfer via manifold embedded distribution alignment. [24] develop an energy distribution-based classifier by which the confidence target data are detected. In all the aforementioned methods, the source data is indispensable because the labeled samples are used to formulate domain knowledge explicitly (e.g., probability, geometrical structure, or energy). When the labeled source domain data are not available, these traditional UDA methods fail.

B. Source Data-absent Unsupervised Domain Adaptation

Current solutions for the SAUDA problem mainly follow three clues. The first one is to convert model adaptation without source data to a classic UDA setting by faking a source domain. [4] incorporated a conditional generative adversarial net to explore the potential of unlabeled target data. The second focuses on mining transferable factors that are suitable for both domains. [25] supposed that a sample and its exemplar classifier (SVM) satisfy a certain mapping relationship. Following this idea, this method learned the mapping on the source domain and predicted the classifier for each target sample to perform an individual classification. [7] used the nearest centroid classifier to represent the subspace where the target domain can be transferred from the source domain in a moderate way. As it features no end-to-end training, this kind of method may not work well enough in practice. The third provides the end-to-end solution. This kind of method performs self-training with a pre-trained source model to bypass the absence of the source domain and the label information of the target domain. [5] developed a general end-to-end method following deep clustering and a hypothesis transfer framework to implement an implicit alignment from the target data to the probability distribution of the source domain. In the method, information maximization (IM) [26] and pseudo-labels, generated by self-labelling, were used to supervise the self-training. [6] canceled the self-labelling operation and newly added a classifier to offer the semantic guidance for the right move. These two methods obtained outstanding results, however, they ignored the fact that the geometric structure between data can provide meaningful context.

C. Deep Clustering

Deep clustering (DC) [27], [28], [29], [30] performs deep network learning together with discovering the data labels unlike conventional clustering performed on fixed features [31], [32]. Essentially, it is a process of simultaneous clustering and representation learning. Combining cross-entropy minimization and a k-means clustering algorithm, the recent DeepCluster [8] method first proposed a simple but effective implementation. Most recently, [33] and [34] boosted the framework developed by DeepCluster. [33] introduced a data equipartition constraint to address the problem of all data

points mapped to the same cluster. [34] provided a concise form without k-means-based pseudo-label where the augmentation data's logits are used as the self-supervision. Besides the unsupervised learning problem on the vast dataset, such as ImageNet, various attempts have been made to solve the UDA problem. [35] leveraged spherical k-means clustering to improve the feature alignment. The work in [36] introduced an auxiliary counterpart to uncover the intrinsic discrimination among target data to minimize the KL divergence between the introduced one and the predictive label distribution of the network. For SAUDA, DC also achieved excellent results, for example, [5] and [6] that we review in the last part. All of these methods mentioned above only focus on learning the representation of data from single samples. The extra constraints hidden in the geometric structure between data were not well exploited.

III. PRELIMINARY

A. Problem Formulation

Given two domains with different probability distributions, i.e., source domain \mathcal{S} and target domain \mathcal{T} , where \mathcal{S} contains n_s labeled samples while \mathcal{T} has n_t unlabeled data. Both labeled and unlabeled samples share the same K categories. Let $\mathcal{X}_s = \{\mathbf{x}_i^s\}_{i=1}^{n_s}$ and $\mathcal{Y}_s = \{y_i^s\}_{i=1}^{n_s}$ be the source samples and their labels where y_i^s is the label of \mathbf{x}_i^s . Let $\mathcal{X}_t = \{\mathbf{x}_i^t\}_{i=1}^{n_t}$ and $\mathcal{Y}_t = \{y_i^t\}_{i=1}^{n_t}$ be the target samples and their labels.

Traditional UDA intends to conduct a K -way classification on the target domain with the labeled source data and the unlabeled target data. In contrast, SAUDA tries to build a target function (model) $f_t : \mathcal{X}_t \rightarrow \mathcal{Y}_t$ for the classification task, while only \mathcal{X}_t and a pre-obtained source function (model) $f_s : \mathcal{X}_s \rightarrow \mathcal{Y}_s$ are available.

B. Semantic Consistency on Nearest Neighborhood (SCNNH)

Much work has shown that the geometric structure between data is beneficial for unsupervised learning. An example of this are the pseudo-labels generated by clustering with global geometric information. The local geometry and semantics (class information) of data are closely related. Self-learning is known as an important way for babies to gain knowledge through experience. Research has found that babies will use a simple strategy, named category learning [37], [38], to supervise their self-learning. Specifically, babies tend to classify a new object into the category that its most similar object belongs. When the semantics of the most similar object is reliable, babies can correctly identify the new object by this strategy.

Inspired by the cognition mechanism introduced above, we propose a new semantic constraint, named semantic consistency on the nearest neighborhood (SCNNH): *the samples in NNH should have the same semantic representation as close to the true category as possible*. The constraint can promote the robust clustering pursued by this paper in two folds: **(i)** the constraint is confined to the local geometry of NNH that helps us to carry out clustering taking NNH as the basic clustering unit, and **(ii)** the consistency makes the NNH samples all move to the same cluster center. To implement the SCNNH constraint, we should address two essentials. One is to

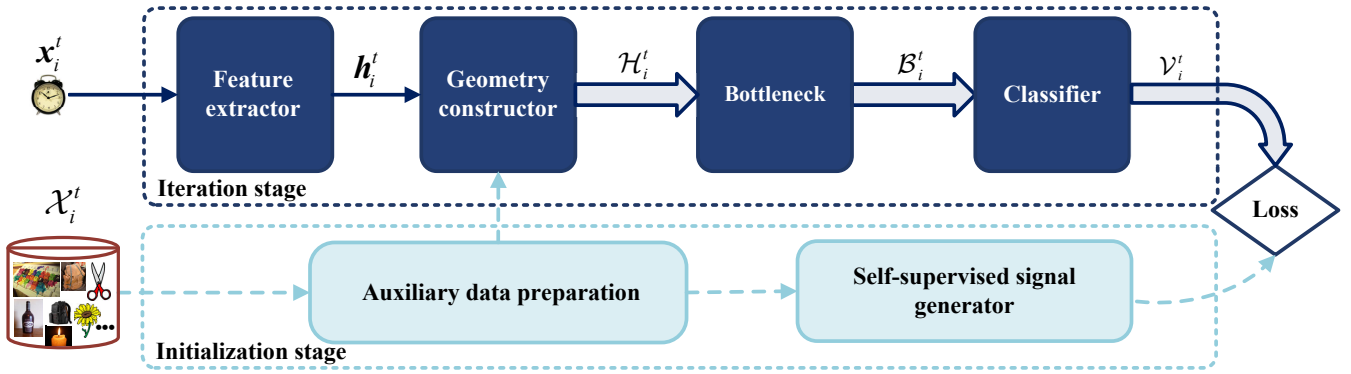


Fig. 2: Our pipeline for model adaptation. **Top:** This branch contains the target model with a geometry construction module, i.e., geometry constructor, and works in the iteration stage of an epoch. **Bottom:** This branch includes the two supporting modules working in the initialization stage. To assist the self-training in the target model, the generated auxiliary data help the geometry building and the self-supervised signal generation. And the generated self-supervised signal offers semantic regulation.

construct proper NNH, while another is to model the semantic consistency. Focusing on these two issues, we develop the adaptation method, as shown in the next section.

IV. METHODOLOGY

In this section, we introduce the framework of the proposed method, followed by the details of the modules in the framework and the regularization method.

A. Model Adaptation Framework

According to the manner of a hypothesis transfer framework, our solution for SAUDA consists of two phases. The first one is the pre-training phase to train the source model, and the second is the adaptation phase to transfer the obtained source model to the target domain.

Pre-training Phase. We take a deep network as the source model. Specifically, we parameterize a feature extractor $u_s(\cdot; \theta_s)$, a bottleneck $g_s(\cdot; \phi_s)$, and a classifier $c_s(\cdot; \psi_s)$ as the network where $\{\theta_s, \phi_s, \psi_s\}$ collects the network parameters. We also use $c_s \circ g_s \circ u_s$ to denote the source model f_s . For input instance x_i^s , this network finally outputs a probability vector $\mathbf{p}_i^s = \text{softmax}(c_s \circ g_s \circ u_s(x_i^s)) \in [0, 1]$.

In this model, the feature extractor is a deep architecture initiated by a pre-trained deep model, for example, ResNet [39]. The bottleneck consists of a batch-normalization layer and a fully-connect layer, while the classifier comprises a weight-normalization layer and a fully-connect layer. We train the source model via optimizing the objective as follows.

$$\min_{\{\theta_s, \phi_s, \psi_s\}} \mathcal{L}_{c_s \circ g_s \circ u_s}^s = -\frac{1}{n_s} \sum_{i=1}^{n_s} \sum_{k=1}^K \bar{l}_{i,k}^s \log \mathbf{p}_{i,k}^s. \quad (1)$$

In Eqn. (1), $\mathbf{p}_{i,k}^s$ is the k -th element of \mathbf{p}_i^s ; $\bar{l}_{i,k}^s$ is the k -th element of $\bar{\mathbf{l}}_i^s = (1 - \gamma) \mathbf{l}_i^s + \gamma/K$, i.e., the smooth label [40], where \mathbf{l}_i^s is a one-hot encoding of label y_i^s .

Adaptation Phase. In this phase, we learn f_t by self-training a target model in an epoch-wise manner. Fig. 2 presents the pipeline for this self-training. The target model has a similar structure as the source model except for a newly

introduced module named geometry constructor. As shown at the top of Fig. 2, the target model includes four modules. They are **(i)** a deep feature extractor $u_t(\cdot; \theta_t)$, **(ii)** the geometry constructor, **(iii)** a bottleneck $g_t(\cdot; \phi_t)$, and **(iv)** a classifier $c_t(\cdot; \psi_t)$ where $\{\theta_t, \phi_t, \psi_t\}$ are the model parameters. We also write them as $u_t(\cdot)$, $g_t(\cdot)$ and $c_t(\cdot)$ for simplicity and use $c_t \circ g_t \circ u_t$ to denote the target model f_t . To implement the self-training and geometry building, as shown at the bottom of Fig. 2, we propose another branch, including an auxiliary data preparation module and a self-supervised signal generator.

Algorithm 1 Pseudo-code of the target model training.

Input: Pre-trained source model $f_s(\theta_s, \phi_s, \psi_s)$; target samples \mathcal{X}_t ; max epoch number T_m ; max iteration number N_b of each epoch.

Initialization: Initialize $\{\theta_t, \phi_t, \psi_t\}$ using $\{\theta_s, \phi_s, \psi_s\}$.

- 1: **for** Epoch = 1 to T_m **do**
 - 2: Generate auxiliary data by the module of auxiliary data preparation.
 - 3: Generate semantic-fused pseudo-labels for \mathcal{X}_t by the self-supervised signal generator.
 - 4: **for** Iter = 1 to N_b **do**
 - 5: Sample a batch and get their pseudo-labels.
 - 6: Construct dynamical NNH for the data in this batch by the geometry constructor.
 - 7: Update model parameters $\{\theta_t, \phi_t, \psi_t\}$ by optimizing the SCNNH-based objective.
 - 8: **end for**
 - 9: **end for**
-

The modules mentioned above work in two parallel stages of a training epoch. In the initialization stage, the self-supervised signal generator conducts self-labelling to output semantic-fused pseudo-labels for all target data. The auxiliary data preparation outputs data to facilitate the other two modules, including the geometry constructor and the self-supervised signal generator. As for the iteration stage, these modules in the target model transform input data from pixel space to the logits space, as shown at the top of Fig. 2. Firstly,

the deep feature extractor transforms \mathbf{x}_i^t into a deep feature \mathbf{h}_i^t . Secondly, the geometry constructor builds NNH for all data at the deep feature space. Using this module, we switch the clustering unit from individual data \mathbf{h}_i^t to its NNH. We use $\mathcal{H}_i^t = \{\mathbf{h}_i^t, \mathbf{h}_{in}^t\}$ to denote NNH where \mathbf{h}_{in}^t is the nearest neighbor of \mathbf{h}_i^t . Thirdly, the bottleneck maps the constructed NNH \mathcal{H}_i^t into a low-dimensional feature space. We use $\mathcal{B}_i^t = \{\mathbf{b}_i^t, \mathbf{b}_{in}^t\} = \{g_t(\mathbf{h}_i^t), g_t(\mathbf{h}_{in}^t)\}$ to represent the output of g_t . Finally, the classifier further maps \mathcal{B}_i^t into a final semantic space. We use $\mathcal{V}_i^t = \{\mathbf{v}_i^t, \mathbf{v}_{in}^t\} = \{c_t(\mathbf{b}_i^t), c_t(\mathbf{b}_{in}^t)\}$ to represent the ending output.

Alg. 1 summarizes the training process of the target model f_t . Before training, we initialize f_t using the pre-trained source model f_s . Specifically, we use u_s, g_s and c_s in f_s to initialize the corresponding parts, i.e., u_t, g_t and c_t , of the target model, respectively. Subsequently, we freeze the parameters of c_t during the succeeding training. After completing the model initialization, we start the self-training, which runs in an epoch-wise manner.

Note: In the inference time, we do not need to keep the full training set in memory to construct and update the local neighborhood for every incoming input. We simply obtain the category prediction by passing the input data through the three network modules, i.e., u_t, g_t and c_t .

B. Auxiliary Data Preparation

At the beginning of an epoch, we prepare the auxiliary data by making all target data go through the target model. For all target data $\{\mathbf{x}_i^t\}_{i=1}^{n_t}$, the target model first outputs the deep features $\{\mathbf{h}_i^t\}_{i=1}^{n_t}$, then outputs the low-dimensional features $\{\mathbf{b}_i^t\}_{i=1}^{n_t}$, and finally outputs the logits features $\{\mathbf{v}_i^t\}_{i=1}^{n_t}$. Considering that the obtained information is frozen during the upcoming epoch, we rewrite these features as $\{\bar{\mathbf{h}}_i^t\}_{i=1}^{n_t}$, $\{\bar{\mathbf{b}}_i^t\}_{i=1}^{n_t}$ and $\{\bar{\mathbf{v}}_i^t\}_{i=1}^{n_t}$ to indicate this distinction. For simplicity, we also collectively write them as $\bar{\mathbf{H}}_t, \bar{\mathbf{B}}_t$, and $\bar{\mathbf{V}}_t$, respectively.

C. Semantic-Fused Self-labelling

The semantic-fused self-labelling is to output the semantic-fused pseudo-labels. We adopt two steps to generate this kind of pseudo-labels including 1) NNH construction and 2) pseudo-labels generation.

Static NNH construction. In this step, we use a similarity-comparison-based method over the pre-computed deep features $\bar{\mathbf{H}}_t$ to find the nearest neighbor of $\bar{\mathbf{h}}_i^t$ and build the NNH. Because this geometry building is only executed once in the initiation stage, we term this construction as the static NNH construction.

Without loss of generality, for given data \mathbf{u} , we use $\mathbf{u}_{in} = F(\mathbf{u}; U)$ to represent its nearest neighbor detected in set U . We make this function $F(\cdot; \cdot)$ equivalent to an optimization problem formulated by Eqn. (2) where $D_{sim}(\cdot, \cdot)$ is the cosine distance function computing the similarity of two vectors.

$$\begin{aligned} \mathbf{u}_{in} &= \mathbf{u}_{i'}, \quad i' = \arg \min_i D_{sim}(\mathbf{u}, \mathbf{u}_i), \\ \text{s.t. } & i = 1, 2, \dots, |U|; \mathbf{u} \neq \mathbf{u}_i; \mathbf{u}_i, \mathbf{u}_{i'} \in U. \end{aligned} \quad (2)$$

Thus, we obtain $\bar{\mathbf{h}}_i^t$'s nearest neighbor $\bar{\mathbf{h}}_{in}^t = F(\bar{\mathbf{h}}_i^t; \bar{\mathbf{H}}_t)$ using the method represented by Eqn. (2) and build the NNH on $\bar{\mathbf{H}}_t$, denoted by $\bar{\mathcal{H}}_i^t = \{\bar{\mathbf{h}}_i^t, \bar{\mathbf{h}}_{in}^t\}$.

Pseudo-label generation. This step performs a semantic fusion on $\bar{\mathcal{H}}_i^t$. To facilitate the semantic fusion, we firstly give the method to compute a similarity-based logits of data using the pre-obtained features $\bar{\mathbf{B}}_t$ and $\bar{\mathbf{V}}_t$. We arrive at the similarity-based logits $\bar{\mathbf{q}}_i^t$ of any target data \mathbf{x}_i^t by the following computation.

$$\bar{\mathbf{q}}_i^t = \frac{1}{2} \left(1 + \frac{\bar{\mathbf{b}}_i^{t\top} \boldsymbol{\mu}_k}{\|\bar{\mathbf{b}}_i^t\| \|\boldsymbol{\mu}_k\|} \right) \in [0, 1], \quad \bar{\mathbf{b}}_i^t \in \bar{\mathbf{B}}_t. \quad (3)$$

In Eqn. (3), we perform a weighted k-means clustering over $\bar{\mathbf{B}}_t$ to get $\boldsymbol{\mu}_k$, the k -th cluster centroid. Let $\{\bar{\mathbf{p}}_i^t\}_{i=1}^{n_t}$ be the probability vectors of $\{\bar{\mathbf{v}}_i^t\}_{i=1}^{n_t}$, i.e., $\bar{\mathbf{V}}_t$, after a softmax operation. The computation of $\boldsymbol{\mu}_k$ is expressed to the equation (4) where $\bar{p}_{i,k}$ is the k -th element of $\bar{\mathbf{p}}_i$.

$$\boldsymbol{\mu}_k = \frac{\sum_{i=1}^{n_t} \bar{p}_{i,k} \bar{\mathbf{b}}_i^t}{\sum_{i=1}^{n_t} \bar{p}_{i,k}}, \quad \bar{\mathbf{b}}_i^t \in \bar{\mathbf{B}}_t. \quad (4)$$

It is known that $\bar{\mathbf{b}}_i^t$ and $\bar{\mathbf{h}}_i^t$ satisfy the mapping of g_t , such that, using the method introduced above, we can get $\bar{\mathbf{Q}}_i^t = \{\bar{\mathbf{q}}_i^t, \bar{\mathbf{q}}_{in}^t\}$ that is the similarity-based logits of $\bar{\mathcal{H}}_i^t$. Based on $\bar{\mathbf{Q}}_i^t$, we perform a dynamical fusion-based method to generate the pseudo-label. Assigning \bar{y}_i^t as the pseudo-label of target data \mathbf{x}_i^t , we get it by optimizing the objective as follows.

$$\begin{aligned} \min_k M_k \left(\bar{\mathbf{Q}}_i^t \right) &= \lambda_k \bar{q}_{i,k}^t + (1 - \lambda_k) \bar{q}_{in,k}^t, \\ \text{s.t. } & k = 1, 2, \dots, K, \end{aligned} \quad (5)$$

where $M_k(\cdot)$ stands for the k -th element of function $M(\cdot)$ output, $\bar{q}_{i,k}^t$ and $\bar{q}_{in,k}^t$ are the k -th element of $\bar{\mathbf{q}}_i^t$ and $\bar{\mathbf{q}}_{in}^t$ respectively, λ_k is the k -th element of random vector $\lambda \sim N(\alpha, \delta)$, in which $\delta = 1 - \alpha$. During the consecutive iteration stage, we fix these pseudo-labels and take them as a self-supervised signal to regulate the self-training.

D. Dynamical NNH Construction

In the iteration stage of an epoch, we dynamically build NNH for every input instance based on the pre-computed deep feature $\bar{\mathbf{H}}_t$. Our idea also is to construct NNH by detecting the nearest neighbor of the input instance from $\bar{\mathbf{H}}_t$. For an input instance \mathbf{x}_i^t whose deep feature is \mathbf{h}_i^t , we form its NNH by the following steps.

- Find the nearest neighbor $\mathbf{h}_{in}^t = F(\mathbf{h}_i^t, \bar{\mathbf{H}}_t)$.
- Construct the NNH \mathcal{H}_i^t combining \mathbf{h}_i^t and \mathbf{h}_{in}^t .

As shown in Fig. 2, after we complete the NNH geometry building, the subsequent calculations are performed based on the local geometry instead of individual data. In other words, we perform a switch for the fundamental clustering unit.

Remarks. The NNH construction in the iteration stage is different from the operation in the initiation stage (refer to the static NNH construction operation in Section IV-C). Due to the update of model parameters, for instance \mathbf{x}_i^t , the target model outputs different deep features \mathbf{h}_i^t that lead to the various nearest neighbors \mathbf{h}_{in}^t . Therefore, we term the construction in the iteration stage as a dynamical NNH construction.

E. SCNNH-based Regularization for Model Adaptation

To drive NNH-based deep clustering, inspired by [5], this paper adopts a joint objective represented by Eqn. (6) to regulate the clustering.

$$\min_{\{\theta_t, \phi_t\}} \mathcal{L}_{g_t \circ u_t}^t(\mathcal{H}_i^t) = \mathcal{L}_{im}^t(\mathcal{H}_i^t) + \beta \mathcal{L}_{ss}^t(\mathcal{H}_i^t). \quad (6)$$

In the Eqn. above, \mathcal{L}_{im}^t is an NNH-based information maximization (IM) [26] regularization, \mathcal{L}_{ss}^t is an NNH-based self-supervised regularization, β is a trade-off parameter. In the clustering process, \mathcal{L}_{im}^t mainly drives global clustering while \mathcal{L}_{ss}^t provides category-based adjustment to correct the wrong move. Different from [5], our objective is built on NNH instead of individual data.

This paper proposes the SCNNH constraint, introduced in Section III-B, to encourage robust deep clustering taking NNH as the fundamental unit. Aiming at the *same semantic representation on NNH*, we implement this constraint in both regularizations \mathcal{L}_{im}^t and \mathcal{L}_{ss}^t . For input instance x_i^t , the target model outputs its NNH \mathcal{H}_i^t , and finally outputs \mathcal{V}_i^t . We write the probability vectors of \mathcal{V}_i^t as $\mathbf{P}_i^t = \{\mathbf{p}_i^t, \mathbf{p}_{in}^t\}$ after the softmax operation. To ensure the data in NNH have similar semantics, we make them move concurrently to a specific cluster centroid, such that NNH moves as a whole. To achieve this goal, we perform a semantic fusion operation $G(\mathbf{P}_i^t)$, as shown below.

$$G(\mathbf{P}_i^t) = \omega_i \mathbf{p}_i^t + \omega_{in} \mathbf{p}_{in}^t, \quad (7)$$

where ω_i and ω_{in} are weight parameters. Let $\hat{\mathbf{p}}_i^t = G(\mathbf{P}_i^t)$, we formulate the IM term \mathcal{L}_{im}^t by the following objective.

$$\mathcal{L}_{im}^t(\mathcal{H}_i^t) = -\frac{1}{n_t} \sum_{i=1}^{n_t} \sum_{k=1}^K \hat{p}_{i,k}^t \log \hat{p}_{i,k}^t + \sum_{k=1}^K \varrho_k^t \log \varrho_k^t, \quad (8)$$

where $\hat{p}_{i,k}^t$ is the k -th element of the fused probability vector $\hat{\mathbf{p}}_i^t$, $\varrho_k^t = \frac{1}{n_t} \sum_{i=1}^{n_t} \hat{p}_{i,k}^t$ is a mean in the k -th dimension over the dataset. In Eqn. 8, the first term is an information entropy minimization that ensures clustering of NNH and the second term balances cluster assignments that encourage aggregation diversity over all clusters.

We achieve the semantic consistency of the data in NNH through enforcing the move of NNH, as represented in \mathcal{L}_{im}^t above. However, this IM regularization cannot absolutely guarantee a move to the true category of the input instance. Therefore, we use the pseudo-labels to impose a category guidance. To this end, we introduce the self-supervised regularization \mathcal{L}_{ss}^t formulated by Eqn. (9).

$$\begin{aligned} \mathcal{L}_{ss}^t(\mathcal{H}_i^t) = & -\eta_i \left(\frac{1}{n_t} \sum_{i=1}^{n_t} \sum_{k=1}^K \mathbb{I}[k = \bar{y}_i^t] \log p_{i,k}^t \right) \\ & - \eta_{in} \left(\frac{1}{n_t} \sum_{i=1}^{n_t} \sum_{k=1}^K \mathbb{I}[k = \bar{y}_i^t] \log p_{in,k}^t \right), \end{aligned} \quad (9)$$

where η_i and η_{in} are weight parameters, $\mathbb{I}[\cdot]$ is the function of indicator, $p_{i,k}^t$ and $p_{in,k}^t$ are the k -th elements of probability vectors \mathbf{p}_i^t and \mathbf{p}_{in}^t respectively.

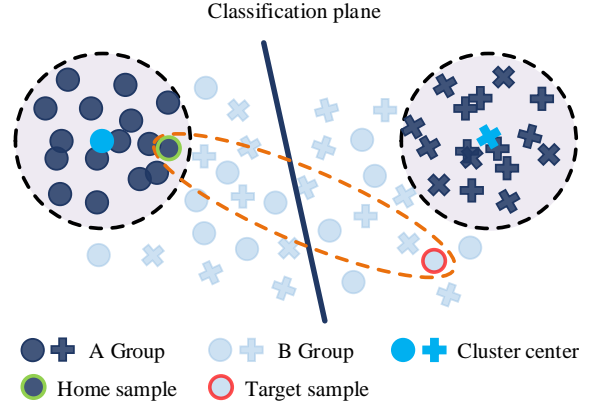


Fig. 3: Structure of SHNNH geometry.

V. DEEP CLUSTERING BASED ON SEMANTIC HYPER-NEAREST NEIGHBORHOOD

In category learning, the similarity-based cognition strategy will work well when the semantics of the most similar object is reliable. However, in the NNH based on the spatial information, as represented in Section IV-C, we suppose all nearest neighbors' semantic credibilities are equal. To better mimic the working mechanism in category learning, we propose a more SCNNH-compliant version of NNH by introducing semantic credibility constraints. We term this new structure as semantic hyper-nearest neighborhood (SHNNH). In the following, we firstly introduce the structure of SHNNH, followed by its construction method. In the end, we present how to extend our method to this new geometry.

A. Semantic Hyper-nearest Neighborhood (SHNNH)

Using the feature extractor u_s to map the target data into the deep feature space, we find that the obtained feature data has particular clustering (discriminative) characteristics (see Fig. 3), benefiting from the powerful feature extraction capabilities of deep networks. For one specific cluster, we can roughly divide the feature samples into two categories: **i)** data located near the cluster centers (A group) and **ii)** samples far away from the centers (B group). Some samples in the B group closely distribute over the classification plane. This phenomenon implies that the semantic information of the A group is more credible than that of the B group. Therefore, we plan to select samples from the A group to construct NNH.

Suppose samples in the A group and B group (see Fig. 3) are respectively confident and unconfident data. We model the self-learning process in category learning by defining a hyper-local geometry, i.e., SHNNH (marked by an orange dotted oval in Fig. 3). We form SHNNH by a target sample (marked by a red circle) and a home sample (marked by a green circle). In this geometry, the home sample is the high-confidence data most similar to the target sample.

B. SHNNH Geometry Construction

As with previous NNH only constructed by the spatial information, we build SHNNH by detecting the home sample that

we implement by two steps in turn: (i) confident group splitting and (ii) home sample detection. Using these in combination, we find the most similar data with high confidence.

Confident Group Splitting. This operation is performed in the initialization stage. In this step, based on the information entropy of data, we split the target data into a confident group \mathcal{C}^e and unconfident group in the deep feature space.

Suppose that the auxiliary information, including the deep features $\bar{\mathbf{H}}_t$, the low-dimensional features $\bar{\mathbf{B}}_t$ and the logits feature $\bar{\mathbf{V}}_t$, is pre-computed. After the softmax operation, the final probability vector is $\{\bar{\mathbf{p}}_i^t\}_{i=1}^{n_t}$. We adopt a simple strategy to obtain the confident group according to the following equation.

$$\bar{\mathcal{C}}^e = \left\{ \bar{\mathbf{h}}_i^t \mid \text{ent}_i^t < \gamma_e \right\}, \bar{\mathbf{h}}_i^t \in \bar{\mathbf{H}}_t \quad (10)$$

where $\text{ent}_i^t = -\sum_{k=1}^K \bar{\mathbf{p}}_{i,k}^t \log \bar{\mathbf{p}}_{i,k}^t$ is the information entropy corresponding to $\bar{\mathbf{h}}_i^t$, threshold γ_e is the median value of the entropy over all target data.

Also, to obtain more credible grouping, we perform another splitting strategy based on the minimum distance to the cluster centroid in the low-dimensional feature space. We denote the new confident group as \mathcal{C}^d . The new splitting strategy contains the two following steps.

Firstly, we conduct a weighted k-means clustering and get K cluster centroids and compute the similarity-based logits of all target data $\{\bar{\mathbf{q}}_i^t\}_{i=1}^{n_t}$ according to Eqn. (3) and Eqn. (4). Secondly, we obtain the new confident group by Eqn. (11).

$$\bar{\mathcal{C}}^d = \left\{ \bar{\mathbf{h}}_i^t \mid \bar{d}_i < \gamma_d \right\}, \bar{\mathbf{h}}_i^t \in \bar{\mathbf{H}}_t \quad (11)$$

$$\bar{d}_i = \min(\bar{\mathbf{q}}_i),$$

where $\min(\cdot)$ is a function that outputs the minimum of the input vector, and threshold γ_d is also the median value of a measure-set $\bar{\mathbf{D}}_t = \{\bar{d}_i\}_{i=1}^{n_t}$. Combining $\bar{\mathcal{C}}^e$ and $\bar{\mathcal{C}}^d$, we get the final confident group $\bar{\mathcal{C}}$ by conducting an intersection operation represented by Eqn. (12).

$$\bar{\mathcal{C}} = \bar{\mathcal{C}}^e \cap \bar{\mathcal{C}}^d. \quad (12)$$

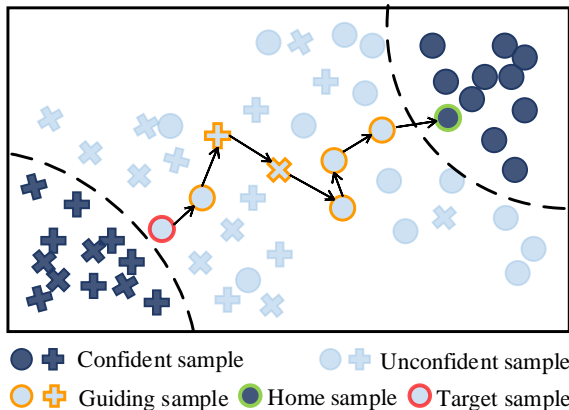


Fig. 4: Illustration of home sample detection by chain-search in the deep feature space.

Home Sample Detection. Without loss of generality, we present our detecting method focusing on the geometry construction in pseudo-label generation. In the implementation, we do not directly find the home sample from the confident group $\bar{\mathcal{C}}$ but propose a chain-search method that fully considers the nearest neighbor constraint.

As shown in Fig. 4, the method starts with a target sample (with a red circle) in the deep feature space. Subsequently, it searches a serial of guiding samples (with an orange circle) one by one without repeating itself, using most-similarity comparison, until the home sample (with a green circle) is detected. In the detection chain, only the ending home samples belong to the confident group.

Given the $(k-1)$ -th guiding sample $\bar{\mathbf{h}}_{ig}^{t(k-1)}$ and a temporary set \mathbf{I}_k storing the found guiding samples. We formulate the search over the deep features $\bar{\mathbf{H}}_t$ for the k -th new guiding sample $\bar{\mathbf{h}}_{ig}^{t(k)}$ by the following optimization where $\langle k \rangle$ means the k -th iteration.

$$\bar{\mathbf{h}}_{ig}^{t(k)} = \bar{\mathbf{h}}_{j'}^t, \quad j' = \arg \min_j D_{sim}(\bar{\mathbf{h}}_{ig}^{t(k-1)}, \bar{\mathbf{h}}_j^t), \quad (13)$$

s.t. $j = 1, 2, \dots, n_t; ig \neq j; \bar{\mathbf{h}}_j^t \in \bar{\mathbf{H}}_t; \bar{\mathbf{h}}_j^t \notin \mathbf{I}_k;$

where $D_{sim}(\cdot, \cdot)$ is the cosine distance function. We use function $R(\cdot; \bar{\mathbf{H}}_t, \bar{\mathcal{C}})$ to express the home sample search process in general. For deep feature $\bar{\mathbf{h}}_i^t$, corresponding to any target data \mathbf{x}_i^t , the search for the home sample $\bar{\mathbf{h}}_{ih}^t = R(\bar{\mathbf{h}}_i^t; \bar{\mathbf{H}}_t, \bar{\mathcal{C}})$ can be expressed by Alg. 2.

Algorithm 2 Pseudo-code of home sample detection.

Input: $\bar{\mathbf{h}}_i^t, \bar{\mathbf{H}}_t$ and $\bar{\mathcal{C}}$

Output: $\bar{\mathbf{h}}_{ih}^t$

Initialization: $k = 1, \bar{\mathbf{h}}_{ig}^{t(k-1)} = \bar{\mathbf{h}}_i^t$ and $\mathbf{I}_k = \emptyset$.

1: **do**

2: Find the guiding sample $\bar{\mathbf{h}}_{ig}^{t(k)}$ by Eqn. 13.

3: Add $\bar{\mathbf{h}}_{ig}^{t(k)}$ into set \mathbf{I}_k .

4: Update $\bar{\mathbf{h}}_{ig}^{t(k-1)}$ by $\bar{\mathbf{h}}_{ig}^{t(k-1)} = \bar{\mathbf{h}}_{ig}^{t(k)}$.

5: Update searching counter $k += 1$.

6: **while** $\bar{\mathbf{h}}_{ig}^{t(k)} \notin \bar{\mathcal{C}}$.

7: **return** The home sample $\bar{\mathbf{h}}_{ih}^t = \bar{\mathbf{h}}_{ig}^{t(k)}$.

C. Extending Our Method to SHNNH

As shown in Fig. 2, the adaptation method proposed in this paper is a general framework that we can smoothly extend to the new geometry through simple actions. For SHNNH, we extend our method to this new geometry by updating three modules. Specifically, we update the auxiliary data constructor by integrating the confident group splitting operation introduced in Section V-B. In the meantime, we let $\bar{\mathbf{h}}_{in}^t = \bar{\mathbf{h}}_{ih}^t$ and $\mathbf{h}_{in}^t = \mathbf{h}_{ih}^t = R(\mathbf{h}_i^t; \bar{\mathbf{H}}_t, \bar{\mathcal{C}})$, by which we perform the update for the static NNH construction (see Section IV-C) and the dynamical NNH construction (see Section IV-D), respectively.

In the rest of this paper, we denote the original method, based on the NNH without semantic credibility constraint, as N2DC. Meanwhile, we term the extended method, based on SHNNH, as N2DC-EX for clarity.

VI. EXPERIMENTS

A. Datasets

Office-31 [41] is a small benchmark that has been widely used in visual domain adaptation. The dataset includes 4,652 images of 31 categories, all of which are of real-world objects in an office environment. There are three domains in total, i.e., Amazon (A), Webcam (W), and DSLR (D). Images in (A) are online e-commerce pictures from the Amazon website. (W) consists of low-resolution pictures collected by webcam. (D) are of high-resolution images taken by SLR cameras.

Office-Home [42] is another challenging medium-sized benchmark released in 2017. It is mainly used for visual domain adaptation and consists of 15,500 images, all of which are from a working or family environment. There are 65 categories in total, covering four distinct domains, i.e., Artistic images (Ar), Clipart (Cl), Product images (Pr), and Real-World images (Rw).

VisDA-C [43] is the third dataset used in this paper. Different from Office-31 and Office-Home, the dataset is a large benchmark for visual domain adaptation, including target classification and segmentation, and 12 types of synthetic to real target recognition tasks. The source domain contains 152,397 composite images generated by rendering 3D models, while the target domain has 55,388 real object images from Microsoft COCO.

B. Experimental Settings

Network setting. In experiments, we do not train the source model from scratch. Instead, the feature extractor is transferred from pre-trained deep models. Similar to the work in [15], [44], ResNet-50 is used as the feature extractor in the experiments on small and medium-sized datasets (i.e., Office-31 and Office-Home). For the experiments on VisDA-C, ResNet-101 is adopted as the feature extractor. For the bottleneck and classifier, we adopted the structure proposed in [5], [6]. In the bottleneck and the classifier, the fully-connect layers have a size of 2048×256 and $256 \times K$, respectively, in which K differs from one dataset to another.

Training setting. On all experiments, we adopt the same setting for the hyper-parameter γ , (α, δ) , β , (ω_i, ω_{in}) , and (η_i, η_{in}) . Among these parameters, γ is a weight parameter that indicates the degree of relaxation for the smooth label (see Eqn. (1)). Same as [45], we chose $\gamma = 0.1$. (α, δ) as the mean and variance of the random variable λ used in semantic fusion for pseudo-label generation (see Eqn. (5)). We set $(\alpha, \delta) = (0.85, 0.15)$ to ensure that the fused pseudo-label of NNH contains more semantics from the input instance. β is a trade-off parameter representing the confidence for the self-supervision from the semantic consistency loss \mathcal{L}_{ss}^t (see Eqn. (6)). In this paper, we choose a relaxed value of 0.2 for β . (ω_i, ω_{in}) in Eqn. (7) and (η_i, η_{in}) in Eqn. (9) are weight coefficients representing the effects of the two samples forming the NNH. Due to equal importance to NNH construction, we set them to the same value. Under random seed 2020, we run the codes repeatedly for 10 rounds and then take the average value as the final result.

C. Baseline methods

We carry out the evaluation on three domain adaptation benchmarks mentioned in the previous subsection. To verify the effectiveness of our method, we selected 18 comparison methods and divided them into the following three groups.

- The first group includes 13 state-of-the-art UDA methods requiring access to the source data, i.e., DANN[46], CDAN [15], CAT [47], BSP [48], SAFN [44], SWD [49], ADR [50], TN [51], IA [52], BNM [53], BDG [54], MCC [55] and SRDC [36].
- The second group comprises four state-of-the-art methods for UDA without access to the source data. They are SHOT [5], SFDA [3], MA [4] and BAIT [6].
- The third group includes the pre-trained deep models, namely ResNet-50 and ResNet-101 [39], that are used to initiate the feature extractor of the source model before training on the source domain.

TABLE I: Classification accuracies (%) of 6 transfer tasks on the small Office-31 data set. The bold means the best result, the underline means the second-best result, and **SDA** means Source Data-Absent.

Method ($\mathcal{S} \rightarrow \mathcal{T}$)	SDA	A→D	A→W	D→A	D→W	W→A	W→D	Avg.
ResNet-50 [39]	×	68.9	68.4	62.5	96.7	60.7	99.3	76.1
DANN [46]	×	79.7	82.0	68.2	96.9	67.4	99.1	82.2
CDAN [15]	×	92.9	94.1	71.0	98.6	69.3	100.	87.7
CAT [47]	×	90.8	94.4	72.2	98.0	70.2	100.	87.6
SAFN [44]	×	90.7	90.1	73.0	98.6	70.2	<u>99.8</u>	87.1
BSP [48]	×	93.0	93.3	73.6	98.2	72.6	100.	88.5
TN [51]	×	94.0	<u>95.0</u>	73.4	98.7	74.2	100.	89.3
IA [52]	×	92.1	<u>90.3</u>	75.3	98.7	74.9	<u>99.8</u>	88.8
BNM [53]	×	90.3	91.5	70.9	98.5	71.6	100.	87.1
BDG [54]	×	93.6	93.6	73.2	<u>99.0</u>	72.0	100.	88.5
MCC [55]	×	95.6	95.4	72.6	<u>98.6</u>	73.9	100.	89.4
SRDC [36]	×	<u>95.8</u>	95.7	76.7	99.2	<u>77.1</u>	100.	90.8
SHOT [5]	✓	93.9	91.3	74.1	98.2	74.6	100.	88.7
SFDA [3]	✓	92.2	91.1	71.0	98.2	71.2	99.5	87.2
MA [4]	✓	92.7	93.7	75.3	98.5	77.8	<u>99.8</u>	89.6
BAIT [6]	✓	92.0	94.6	74.6	98.1	75.2	100.	89.1
Source model only	✓	80.7	77.0	60.8	95.1	62.3	98.2	79.0
N2DC (ours)	✓	93.9	89.8	74.7	98.6	74.4	100.	88.6
N2DC-EX (ours)	✓	97.0	93.0	<u>75.4</u>	98.9	75.6	<u>99.8</u>	<u>90.0</u>

D. Quantitative results

Table I~III report the experimental results on the three datasets mentioned above. On Office-31 (Table I), N2DC's performance is close to SHOT. Compared to SHOT, N2DC decreases 0.1% in average accuracy because there is a 1.5% gap in task $A \rightarrow W$. By contrast, N2DC-EX achieves competitive results. Compared to the SAUDA methods, N2DC-EX obtain the best performance in half the tasks and surpass MA, the previous best SAUDA method, by 0.4% on average. In all comparison methods, N2DC-EX obtain the best result in task $A \rightarrow D$ and the second-best result in average accuracy. Considering that the best method SRDC has to work with the source data, we believe that the gap of 0.8% is acceptable. As the results have shown, N2DC and N2DC-EX do not show apparent advantages. We argue that it is reasonable since the small dataset Office-31 cannot support the end-to-end training

TABLE II: Classification accuracies (%) of 12 transfer tasks on the medium Office-Home dataset. The bold means the best result, the underline means the second-best result, and **SDA** means Source Data-Absent.

Method ($S \rightarrow T$)	SDA	Ar→Cl	Ar→Pr	Ar→Rw	Cl→Ar	Cl→Pr	Cl→Rw	Pr→Ar	Pr→Cl	Pr→Rw	Rw→Ar	Rw→Cl	Rw→Pr	Avg.
ResNet-50 [39]	×	34.9	50.0	58.0	37.4	41.9	46.2	38.5	31.2	60.4	53.9	41.2	59.9	46.1
DANN [46]	×	45.6	59.3	70.1	47.0	58.5	60.9	46.1	43.7	68.5	63.2	51.8	76.8	57.6
CDAN [15]	×	50.7	70.6	76.0	57.6	70.0	70.0	57.4	50.9	77.3	70.9	56.7	81.6	65.8
BSP [48]	×	52.0	68.6	76.1	58.0	70.3	70.2	58.6	50.2	77.6	72.2	59.3	81.9	66.3
SAFN [44]	×	52.0	71.7	76.3	64.2	69.9	71.9	63.7	51.4	77.1	70.9	57.1	81.5	67.3
TN [51]	×	50.2	71.4	77.4	59.3	72.7	73.1	61.0	53.1	79.5	71.9	59.0	82.9	67.6
IA [52]	×	56.0	77.9	79.2	64.4	73.1	74.4	64.2	54.2	79.9	71.2	58.1	83.1	69.5
BNM [53]	×	52.3	73.9	80.0	63.3	72.9	74.9	61.7	49.5	79.7	70.5	53.6	82.2	67.9
BDG [54]	×	51.5	73.4	78.7	65.3	71.5	73.7	65.1	49.7	81.1	<u>74.6</u>	55.1	84.8	68.7
SRDC [36]	×	52.3	76.3	81.0	<u>69.5</u>	76.2	78.0	68.7	53.8	81.7	76.3	57.1	85.0	71.3
SHOT [5]	✓	56.6	78.0	80.6	68.4	78.1	<u>79.4</u>	68.0	54.3	82.2	74.3	58.7	84.5	71.9
SFDA [3]	✓	48.4	73.4	76.9	64.3	69.8	71.7	62.7	45.3	76.6	69.8	50.5	79.0	65.7
BAIT [4]	✓	57.4	77.5	82.4	68.0	77.2	75.1	67.1	<u>55.5</u>	81.9	73.9	<u>59.5</u>	84.2	71.6
Source model only	✓	44.0	67.0	73.5	50.7	60.3	63.6	52.6	40.4	73.5	65.7	46.2	78.2	59.6
N2DC (ours)	✓	<u>57.1</u>	<u>79.1</u>	<u>82.1</u>	69.2	<u>78.6</u>	80.3	<u>68.3</u>	54.9	<u>82.4</u>	74.5	59.2	<u>85.1</u>	<u>72.6</u>
N2DC-EX (ours)	✓	57.4	80.0	<u>82.1</u>	69.8	79.6	80.3	68.7	56.5	82.6	74.4	60.4	85.6	73.1

TABLE III: Classification accuracies (%) on the large VisDA-C dataset. The bold means the best result, the underline means the second-best result, and **SDA** means Source Data-Absent.

Method (Syn. → Real)	SDA	plane	bicycl	bus	car	horse	knife	mcycl	person	plant	sktbrd	train	truck	Per-class
ResNet-101 [39]	×	55.1	53.3	61.9	59.1	80.6	17.9	79.7	31.2	81.0	26.5	73.5	8.5	52.4
DANN [46]	×	81.9	77.7	82.8	44.3	81.2	29.5	65.1	28.6	51.9	54.6	82.8	7.8	57.4
ADR [50]	×	94.2	48.5	84.0	72.9	90.1	74.2	92.6	72.5	80.8	61.8	82.2	28.8	73.5
CDAN [15]	×	85.2	66.9	83.0	50.8	84.2	74.9	88.1	74.5	83.4	76.0	81.9	38.0	73.9
IA [52]	×	-	-	-	-	-	-	-	-	-	-	-	-	75.8
BSP [48]	×	92.4	61.0	81.0	57.5	89.0	80.6	90.1	77.0	84.2	77.9	82.1	38.4	75.9
SAFN [44]	×	93.6	61.3	84.1	70.6	94.1	79.0	<u>91.8</u>	79.6	89.9	55.6	89.0	24.4	76.1
SWD [49]	×	90.8	82.5	81.7	70.5	91.7	69.5	<u>86.3</u>	77.5	87.4	63.6	85.6	29.2	76.4
MCC [55]	×	88.7	80.3	80.5	71.5	90.1	93.2	85.0	71.6	89.4	73.8	85.0	36.9	78.8
SHOT [5]	✓	95.0	87.5	81.0	57.6	93.9	94.1	79.3	80.5	90.9	89.8	85.9	<u>57.4</u>	82.7
SFDA [3]	✓	86.9	81.7	<u>84.6</u>	63.9	93.1	91.4	86.6	71.9	84.5	58.2	74.5	<u>42.7</u>	76.7
MA [4]	✓	94.8	73.4	<u>68.8</u>	<u>74.8</u>	93.1	95.4	88.6	84.7	89.1	84.7	83.5	48.1	81.6
BAIT [6]	✓	93.7	83.2	84.5	<u>65.0</u>	92.9	95.4	88.1	80.8	90.0	89.0	84.0	45.3	82.7
Source model only	✓	62.1	21.2	48.8	77.8	63.1	5.0	72.9	25.9	66.1	44.1	80.9	5.3	47.8
N2DC (ours)	✓	<u>95.5</u>	<u>88.1</u>	82.2	58.7	<u>95.5</u>	<u>95.8</u>	85.4	81.4	<u>92.2</u>	91.2	<u>89.7</u>	58.4	<u>84.5</u>
N2DC-EX (ours)	✓	96.6	90.6	87.1	62.6	95.7	96.1	86.0	<u>82.5</u>	93.8	91.3	90.4	56.8	85.8

on our method’s deep network. The results on Office-Home and VisDA-C in the following will confirm our expectation.

On Office-Home (Table II), our methods exceed other methods. Concerning average accuracy, N2DC and N2DC-EX respectively improve by 0.7% and 1.2% compared to the previous second-best method SHOT. N2DC-EX achieves the best results on 10 out of 12 transfer tasks, while N2DC achieves the second-best results on 7 out of 12 tasks. Compared to SRDC that is the best UDA method on Office-31, our two methods have an evident improvement of 1.3% and 1.8%. The results were consistent with our expectations that the larger the dataset used, the better our model’s performance.

Experiments on VisDA-C further verified the above trends. As shown in Table III, both N2DC and N2DC-EX further defeat other methods. N2DC and N2DC-EX obtain best performance on 10 out of 12 tasks in total. N2DC-EX obtains the best results on 8 out of 12 classes and reaches the best accuracy of 85.8% on average. Also, N2DC ranks second on half the

tasks. Compared to the second-best method SHOT and BAIT, the average improvement increases to 1.8% and 3.1% for N2DC and N2DC-EX. Compared to the best SAUDA method MA on Office-31, our two methods improve the average accuracy by at least 2.9% from 81.6%. In our opinion, the evident advantage on VisDA-C is reasonable. On large datasets, due to the increased amount of data, more comprehensive semantic information and more finely portrayed geometric information is available to support our NNH-based deep cluster.

Compared with the SHOT results reported in the three tables, our two methods are equivalent to or better than SHOT on all tasks except for four situations in total. For N2DC, the exceptions include $A \rightarrow W$ and $W \rightarrow A$ on Office-31, and $W \rightarrow D$ on Office-31 and the class ‘truck’ on VisDA-C for N2DC-EX. This indicates that the deep cluster based on NNH is more robust than the cluster taking individual data as the fundamental clustering unit.

Also, N2DC-EX surpasses N2DC on the three datasets in

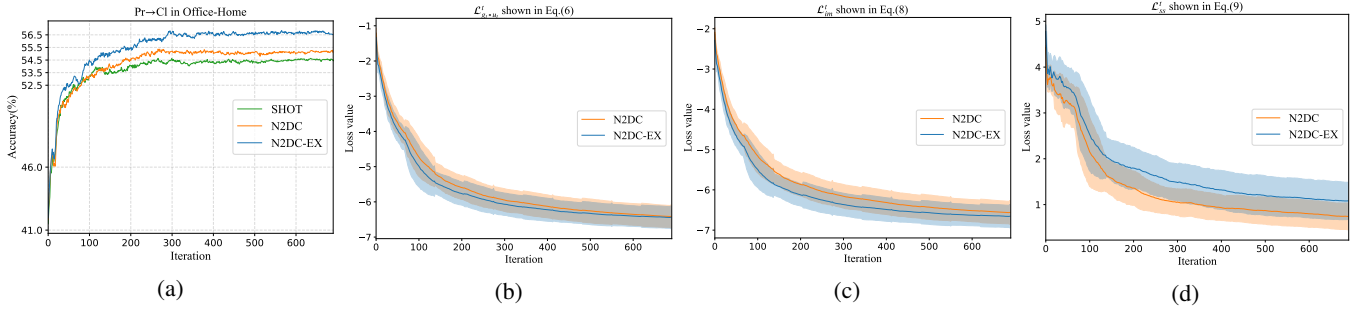


Fig. 5: The accuracy and loss value of our objective during the model adaptation for task Pr→Cl on Office-Home dataset. (a) Accuracies (%) where SHOT is the baseline. (b), (c) and (d) present the loss value of $\mathcal{L}^t_{g_t \circ u_t}$, \mathcal{L}^t_{im} and \mathcal{L}^t_{ss} , respectively.

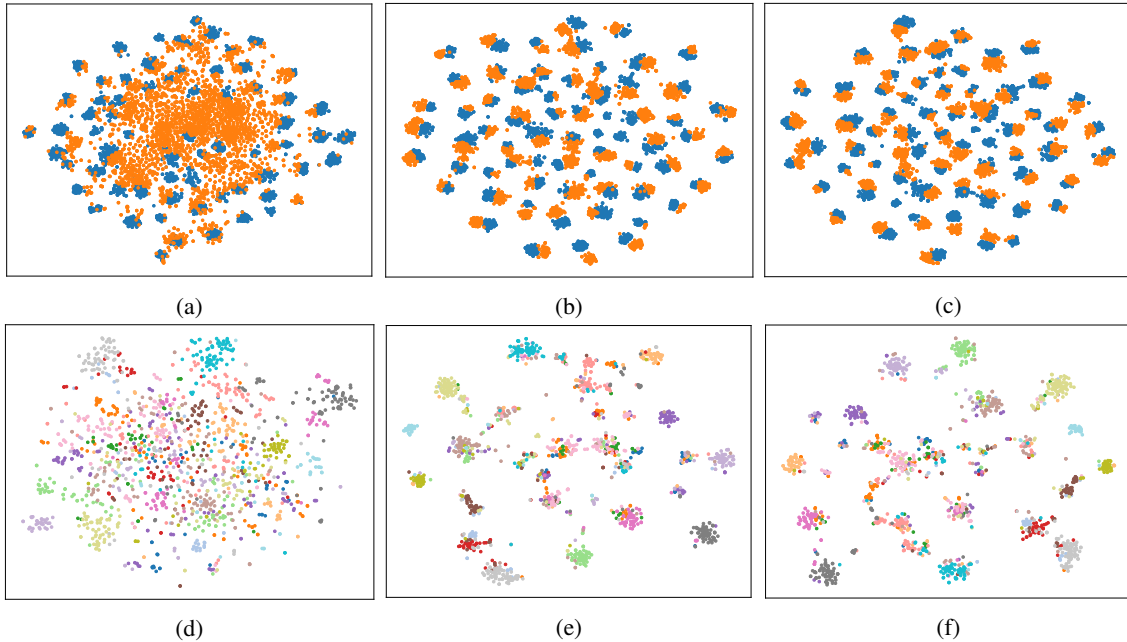


Fig. 6: The t-SNE feature visualizations for task Pr→Cl on Office-Home. (a), (b) and (c) present feature alignment between the source data and the target data by the source model, N2DC and N2DC-EX, respectively. (d), (e) and (f) present deep clustering with category information by the source model, N2DC and N2DC-EX, respectively. In (a), (b) and (c), blue circles denote the features of the absent source data, and orange circles denote the target data’s features. In (d), (e) and (f), only the first 20 categories in each domain are selected for better illustration, and a different color denotes a different category.

average accuracy. On Office-Home, N2DC-EX improves by 0.5% and improves by at least 1.3% on the other two datasets. N2DC beat N2DC-EX in only three situations, including $W \rightarrow D$ on Office-31, $Rw \rightarrow Ar$ on Office-Home and class ‘truck’ on VisDA-C. Besides class ‘truck’ with a gap of 2.4%, there are narrow gaps (up to 0.2%) in two other situations. This comparison between N2DC and N2DC-EX indicates that introducing the semantic credibility used in SHNNH is an effective means to boost our NNH-based deep cluster.

E. Analysis

In this subsection, we analyze our method from the following three aspects for a complete evaluation. To support our analysis, we select two hard transfer tasks as toy experiments, including task Pr→Cl on Office-Home and task W→A on

Office-31. The two tasks have the worst accuracies in their respective datasets.

Training stability. In Fig. 5(a), we display the evolution of the accuracy of our two methods during the model adaptation for task Pr→Cl where SHOT is the baseline. As the iteration increases, N2DC and N2DC-EX stably climb to their best performance. It is also seen that the accuracy of N2DC surpasses SHOT when the iteration is greater than 110, and N2DC-EX beat SHOT at an early phase (at about the iteration of 20). Correspondingly, the loss value of $\mathcal{L}^t_{g_t \circ u_t}$ (Fig. 5(b)), \mathcal{L}^t_{ss} (Fig. 5(c)) and \mathcal{L}^t_{im} (Fig. 5(d)) continuously decreases. This is compliant with the accuracy variety shown in Fig. 5(a).

Feature visualization. Based on the 65-way classification results of task Pr→Cl, we visualize the feature distribution in the low-dimensional feature space by t-SNE tool. As shown in Fig. 6(b)(c), compared to the results obtained by the source

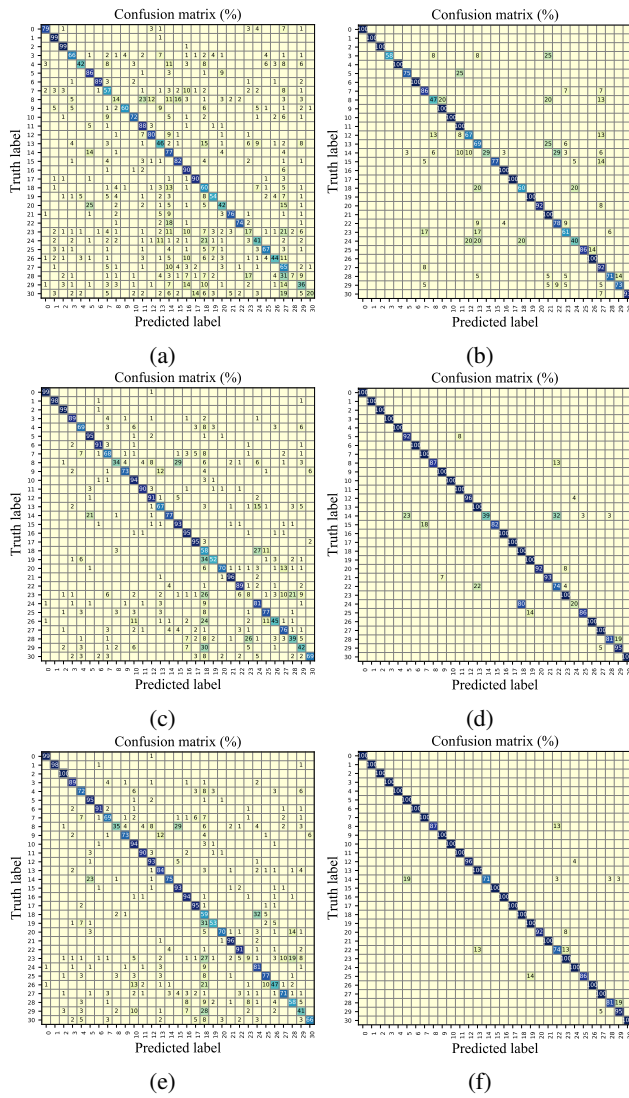


Fig. 7: The confusion matrix for 31-way classification task $W \rightarrow A$ and $A \rightarrow W$ on Office-31 dataset. **Left column:** (a), (c) and (e) present the results of the source model, N2DC and N2DC-EX in task $W \rightarrow A$, respectively. **Right column:** (b), (d) and (f) present the results of the source model, N2DC and N2DC-EX in task $A \rightarrow W$, respectively.

model (Fig. 6(a)), N2DC and N2DC-EX align the target features to the source features. Moreover, the features learned by both N2DC (Fig. 6(e)) and N2DC-EX (Fig. 6(f)) perform a deep clustering with evident category meaning.

Confusion matrix. For a clear view of the figure, we change our experiment to task $W \rightarrow A$ that has half the categories of Office-Home. In addition, we present the results of symmetrical task $A \rightarrow W$ as comparison. Fig. 7 investigates the confusion matrices of the source model, N2DC and N2DC-EX, for the two tasks. From the left column of Fig. 7, we observe that both N2DC and N2DC-EX have evidently fewer misclassifications than the source model on task $W \rightarrow A$. In the right column of Fig. 7, N2DC-EX exposes its advantages over N2DC. From Fig. 7(d)(f), it is seen that N2DC-EX maintains the performance of N2DC in all categories and further improves

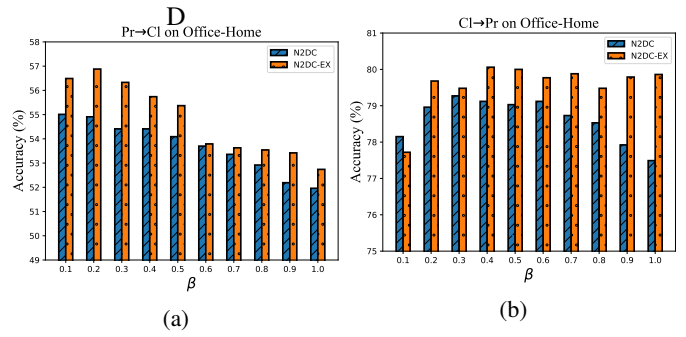


Fig. 8: Performance sensitivity of the trade-off parameter β in our objective. (a) and (b) present the results for hard task $Pr \rightarrow Cl$ and easy task $Cl \rightarrow Pr$ on Office-Home, respectively.

in some hard categories on task $A \rightarrow W$. For example, as shown in the 24-th category, N2DC-EX improves the accuracy from 20% to 100%.

Parameter sensitivity. In our method, there are three vital parameters. The first is β in Eqn. (6) that reflects the adjustment from the self-supervision based on the pseudo-labels. The second is (ω_i, ω_{in}) in Eqn. (7) and (η_i, η_{in}) in Eqn. (9) that determines the impact intensity of the data constructing NNH in the two regularization items \mathcal{L}_{im}^t and \mathcal{L}_{ss}^t , respectively. The third is the random variable λ that describes the semantic fusion on NNH for pseudo-label generation.

We perform a sensitivity analysis of the parameter β in Fig. 8(a) for task $Pr \rightarrow Cl$. N2DC and N2DC-EX respectively reach the best accuracy at $\beta = 0.1$ and $\beta = 0.2$. After that, their accuracies decrease gradually as the value of β increases. This phenomenon shows that for this challenging task, the adjustment from the pseudo-labels is very weak. When the pseudo-labels cannot offer credible category information, an enhancement on self-supervision will deteriorate the final performance. For comparison, we provide the results of an easy case, the symmetry task $Cl \rightarrow Pr$ with an accuracy close to 80%, as shown in Fig. 8(b). N2DC climb to the maximum at a bigger value $\beta = 0.3$ and then gradually decrease because the source model has a much better accuracy than the $Pr \rightarrow Cl$ task that results in pseudo-labels with more credible category information. Different from N2DC, N2DC-EX still reaches a

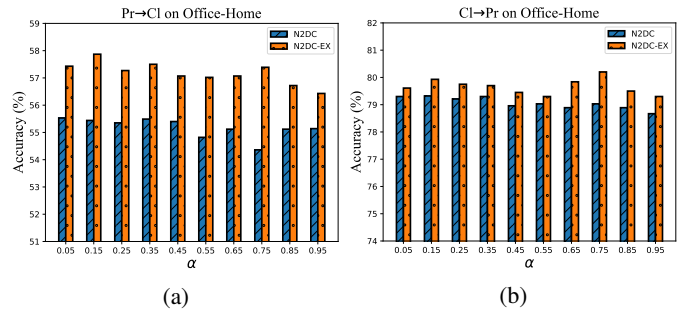


Fig. 9: Performance sensitivity of $\lambda \sim \text{Norm}(\alpha, \delta)$ as the mean α varying with variance $\delta = 1 - \alpha$. (a) and (b) present the results for hard task $Pr \rightarrow Cl$ and easy task $Cl \rightarrow Pr$ on Office-Home, respectively.

robust accuracy at $\beta = 0.2$ as shown in Fig. 8(a) and holds the performance after that. This variation shows that N2DC-EX has a better robustness of parameter β compared to N2DC on the easy task.

Fig. 9 investigates the performance sensitivity of parameter $\lambda \sim \text{Norm}(\alpha, \delta)$ when the mean α changes from 0.05 to 0.95 (the variance $\delta = 1 - \alpha$). On both hard and easy tasks, our two methods do not have a large accuracy decrease. This observation indicates that the semantic fusion in our method for pseudo-label generation is a robust operation.

To better understand the effects of (ω_i, ω_{in}) , and (η_i, η_{in}) , we present their performance sensitivity based on task pair Pr→Cl and Cl→Pr. Letting ω_i and ω_{in} vary from 0.2 to 1.6, the top of Fig. 10 presents the accuracy-matrix of N2DC and N2DC-EX with the obtained 64 parameter pairs on hard task Pr→Cl. For N2DC, the accuracy-matrix in Fig. 10(a) is split by the diagonal, below which these parameter pairs have high accuracies. In contrast, for N2DC-EX, the better zone locates upon the diagonal as shown in Fig. 10(b). Meanwhile, as long as we do not significantly weaken the impact of the input instance, for example, $\omega_i = 0.2$, our method’s performance will not have an evident decrease. In Fig. 10(c)(d), we give the performance sensitivity results for (η_i, η_{in}) . The high-performance zone of N2DC in Fig. 10(c) is upon the diagonal of the accuracy-matrix, especially the region $\eta_{in} > 1$, while N2DC-EX’s high-performance zone is symmetric to the diagonal as shown in Fig. 10(d). Although being smaller than the high accuracy zone of (ω_i, ω_{in}) , the high accuracy region of (η_i, η_{in}) is distributed in patches rather than in isolated parameter pairs.

Similarly, we present the sensitivity results on easy task Cl→Pr at the bottom of Fig. 10. Except for the case shown in Fig.10(b) that has relatively weaker parameter robustness, the other three situations are not sensitive to the changing of parameters. Meanwhile, it is also seen that on the easy task, our method has a better performance sensitivity than on the hard task.

TABLE IV: Ablation study of N2DC on Office-Home dataset. The bold means the best result.

Method	Ablation operation	Avg.
Source model only	—	59.6
N2DC-no-im	Let $\mathcal{L}_{gt \circ u_t}^t = \beta \mathcal{L}_{ss}^t$	69.9
N2DC-no-ss	Let $\mathcal{L}_{gt \circ u_t}^t = \mathcal{L}_{im}^t$	71.5
N2DC-no-NNH-in-im	Set $\omega_{in} = 0$ in Eqn. (7)	72.2
N2DC-no-NNH-in-ss	Set $\eta_{in} = 0$ in Eqn. (9)	72.5
N2DC-no-fused-pl	Fix $\lambda_k = 1.0$ in Eqn. (5)	72.4
N2DC	—	72.6

F. Ablation study

The ablation study is to isolate the effect of the skills adopted in our methods from three aspects. For N2DC, to evaluate the effectiveness of the two regularization components \mathcal{L}_{im}^t and \mathcal{L}_{ss}^t , of our objective, we respectively delete them from the objective and denote the two edited methods by

N2DC-no-im and N2DC-no-ss. To evaluate the effectiveness of changing the clustering unit from individual data to NNH \mathcal{H}_i^t , we give two comparison methods N2DC-no-NNH-in-im and N2DC-no-NNH-in-ss. In N2DC-no-NNH-in-im, the influence of \mathcal{H}_i^t on the \mathcal{L}_{im}^t is eliminated by setting $\omega_{in} = 0$ in Eqn. (7) while in N2DC-no-NNH-in-ss the influence on \mathcal{L}_{ss}^t is canceled by setting $\eta_{in} = 0$ in Eqn. (9). To evaluate the effectiveness of the semantic-fused pseudo-labels, we cancel the fusion operation presented in Eqn. (5) by letting $\lambda_k = 1$ for $k = 1, 2, \dots, K$. We denote the new method by N2DC-no-fused-pl.

TABLE V: Ablation study of N2DC-EX on an Office-Home dataset. The bold means the best result.

Method	Ablation operation	Avg.
Source model only	—	59.6
N2DC-EX-no-im	Let $\mathcal{L}_{gt \circ u_t}^t = \beta \mathcal{L}_{ss}^t$	70.0
N2DC-EX-no-ss	Let $\mathcal{L}_{gt \circ u_t}^t = \mathcal{L}_{im}^t$	72.3
N2DC-EX-no-NNH-in-im	Set $\omega_{in} = 0$ in Eqn. (7)	72.4
N2DC-EX-no-NNH-in-ss	Set $\eta_{in} = 0$ in Eqn. (9)	73.0
N2DC-EX-no-fused-pl	Fix $\lambda_k = 1.0$ in Eqn. (5)	72.9
N2DC-EX-no-chain	Find $\bar{\mathbf{h}}_{ih}^t, \mathbf{h}_{ih}^t$ by $F(\cdot; \bar{\mathcal{C}})$	72.9
N2DC-EX-Ce	Let $\bar{\mathcal{C}} = \bar{\mathcal{C}}^e$	73.1
N2DC-EX-Cd	Let $\bar{\mathcal{C}} = \bar{\mathcal{C}}^d$	73.1
N2DC-EX	—	73.1

Similarly, we carry out all ablation experiments above for N2DC-EX. We use similar notations like N2DC, replacing the ‘N2DC’ with ‘N2DC-EX’, to denote these methods. Also, we add three other experiments. Concretely, to verify the effectiveness of the chain-search method for the home sample detection, we directly find $\bar{\mathbf{h}}_{ih}^t$ and \mathbf{h}_{ih}^t from $\bar{\mathcal{C}}$ using the minimal distance rule presented by $F(\cdot; \bar{\mathcal{C}})$ (refer to Eqn. (2)). We denote this method by N2DC-EX-no-chain. To verify the effectiveness of the confident group detection strategy using intersection, as done in Eqn. (12), we let $\bar{\mathcal{C}} = \bar{\mathcal{C}}^e$ and $\bar{\mathcal{C}} = \bar{\mathcal{C}}^d$ respectively and denote the two methods by N2DC-EX-Ce and N2DC-EX-Cd.

TABLE VI: Supplemental experiment results (Avg.%) for ablation study on Office-31 (OC), Office-Home (OH), and VisDA-C (VC) datasets. The bold means the best result.

Method	OC	OH	VC
N2DC-EX-Ce	89.9	73.1	84.6
N2DC-EX-Cd	89.7	73.1	77.8
N2DC-EX	90.0	73.1	85.8

As reported in Tab. IV and Tab. V, on Office-Home dataset, the performance of all comparison methods decreases by varying degrees as they lack specific algorithm components, compared to the full version, i.e., N2DC and N2DC-EX. This result indicates that the skills aforementioned are all practical. At the same time, we see that the full versions have no improvement compared to N2DC-EX-Ce and N2DC-EX-Cd. To avoid biased evaluation, Tab. VI gives the supplemental

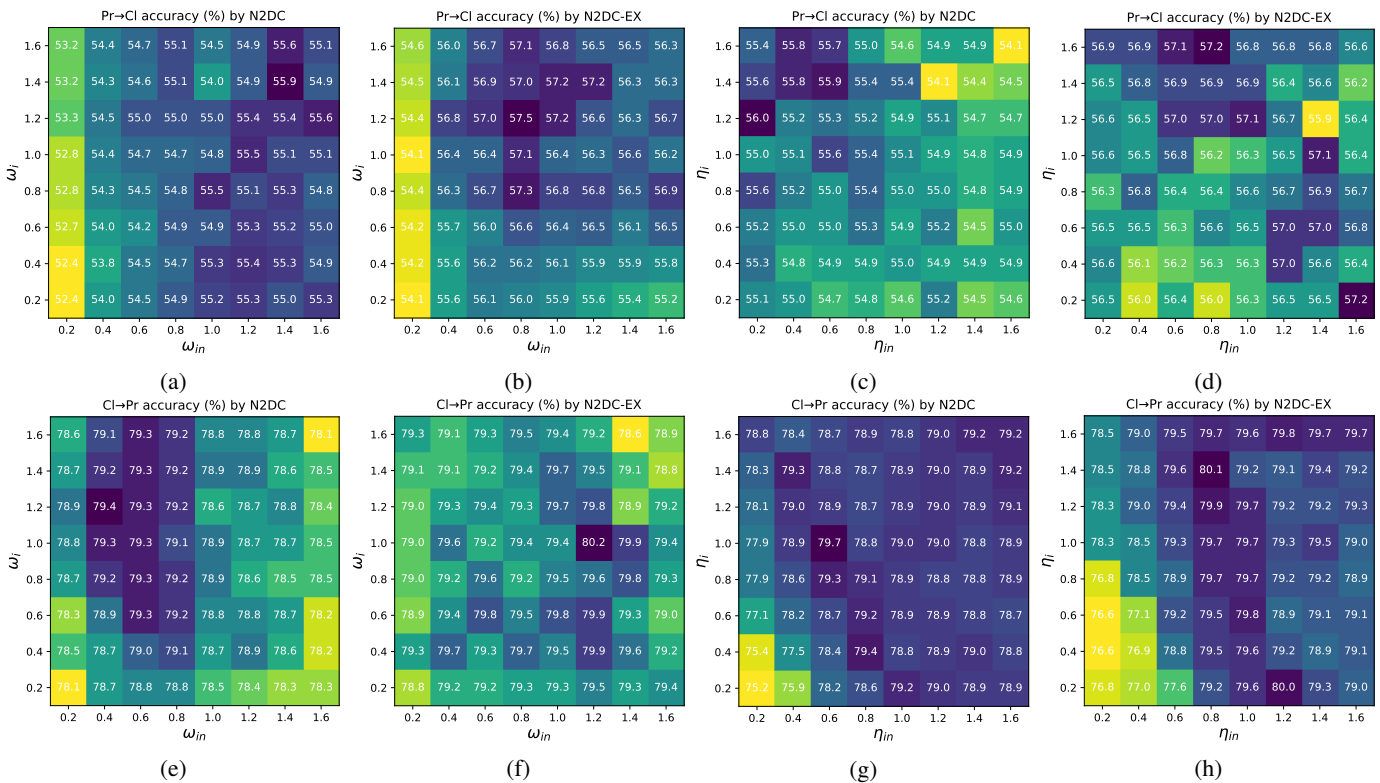


Fig. 10: Performance sensitivity of (ω_i, ω_{in}) and (η_i, η_{in}) . **Top:** the results for task Pr→CI on Office-Home. (a)(b) show the results of our two methods with (ω_i, ω_{in}) varying. The results when (η_i, η_{in}) vary are presented in (c)(d). **Bottom:** the results for task CI→Pr. (e)(f) show the results as (ω_i, ω_{in}) vary while (g)(h) show the results as (η_i, η_{in}) vary.

experiment results of the two comparisons on the other two datasets. On the small Office-31, N2DC-EX surpasses both N2DC-EX-Ce and N2DC-EX-Cd. This advantage of N2DC-EX is more obvious on the large VisDA-C.

VII. CONCLUSION

Deep clustering is a promising method to address the SAUDA problem because it bypasses the absence of source data and the target data's labels by self-supervised learning. However, the individual data-based clustering in the existing DC methods is not a robust process. Aiming at this weakness, we exploit the constraints hidden in the local geometry between data to encourage robust gathering in this paper. To this end, we propose the new semantic constraint SCNNH inspired by a cognitive law named category learning. Focusing on this proposed constraint, we develop a new NNH-based DC method that regards SAUDA as a model adaptation. In the proposed network, i.e., the target model, we add a geometry construction module to switch the basic clustering unit from the individual data to NNH. In the training phase, we initialize the target model with a given source model trained on the labeled source domain. After this, the target model is self-trained using a new objective building upon NNH. As for geometry construction, besides the standard version of NNH that we only construct based on spatial information, we also give an advanced implementation of NNH, i.e., SHNNH. State-of-the-art experiment results on three challenging datasets confirm the effectiveness of our method.

Our method achieves competitive results by only using simple local geometry. This implies that the local geometry of data is meaningful for end-to-end DC methods. We summarize three possibilities for this phenomenon: **(i)** These local structures are inherent constraints, which have robust features and are easy to maintain in non-linear transformation; **(ii)** Compared with other regularizations, the regularization in our method is easy to understand for its obvious geometrical meaning; **(iii)** The local structure is usually linear, thus can be easily modeled.

In our method, the used geometries are all constructed in the Euclidean space. This assumption does not always hold. For example, manifold learning has proved that data locate on a manifold embedded in a high-dimensional Euclidean space. Therefore, our future work will focus on mining geometry with more rich semantic information in more natural data space and form new constraints to boost self-unsupervised learning such as deep clustering.

REFERENCES

- [1] S. J. Pan and Q. Yang, "A survey on transfer learning," *IEEE Trans. Knowl. Data Eng.*, vol. 22, no. 10, pp. 1345–1359, 2009.
- [2] G. Wilson and D. J. Cook, "A survey of unsupervised deep domain adaptation," *ACM Trans. Intell. Syst. Technol.*, vol. 11, no. 5, pp. 1–46, Apr. 2020.
- [3] Y. Kim, S. Hong, D. Cho, H. Park, and P. Panda, "Domain adaptation without source data," *arXiv:2007.01524*, 2020. [Online]. Available: <https://arxiv.org/abs/2007.01524>
- [4] R. Li, Q. Jiao, W. Cao, H.-S. Wong, and S. Wu, "Model adaptation: Unsupervised domain adaptation without source data," in *Proc. IEEE Conf. Comput. Vis. Pattern Recog. (CVPR)*, Jun. 2020, pp. 9638–9647.

- [5] J. Liang, D. Hu, and J. Feng, "Do we really need to access the source data? source hypothesis transfer for unsupervised domain adaptation," in *Proc. Int. Conf. Mach. Learn. (ICML)*, Jul. 2020, pp. 6028–6039.
- [6] S. Yang, Y. Wang, J. van de Weijer, L. Herranz, and S. Jui, "Unsupervised domain adaptation without source data by casting a bait," *arXiv:2010.12427*, 2020. [Online]. Available: <https://arxiv.org/abs/2010.12427>
- [7] J. Liang, R. He, Z. Sun, and T. Tan, "Distant supervised centroid shift: A simple and efficient approach to visual domain adaptation," in *Proc. IEEE Conf. Comput. Vis. Pattern Recog. (CVPR)*, Jun. 2019, pp. 2975–2984.
- [8] M. Caron, P. Bojanowski, A. Joulin, and M. Douze, "Deep clustering for unsupervised learning of visual features," in *Proc. Springer Eur. Conf. Comput. Vis. (ECCV)*, Sep. 2018, pp. 132–149.
- [9] S. Ao, X. Li, and C. X. Ling, "Effective multiclass transfer for hypothesis transfer learning," in *Proc. Adv. Knowledge Discovery and Data Mining Pacific-Asia Conference (PAKDD)*, May. 2017, pp. 64–75.
- [10] A. B. Markman and B. H. Ross, "Category use and category learning," *Psychological bulletin*, vol. 129, no. 4, pp. 592–613, 2003.
- [11] Y. Zhang, Y. Wei, Q. Wu, P. Zhao, S. Niu, J. Huang, and M. Tan, "Collaborative unsupervised domain adaptation for medical image diagnosis," *IEEE Trans. Image Process.*, pp. 7834–7844, 2020.
- [12] Z. Wang, M. Yu, Y. Wei, R. Feris, J. Xiong, W.-M. Hwu, T.-S. Huang, and H. Shi, "Differential treatment for stuff and things: A simple unsupervised domain adaptation method for semantic segmentation," in *Proc. IEEE Conf. Comput. Vis. Pattern Recog. (CVPR)*, Jun. 2020, pp. 12 632–12 641.
- [13] F. Yang, K. Yan, S. Lu, H. Jia, D. Xie, Z. Yu, X. Guo, F. Huang, and W. Gao, "Part-aware progressive unsupervised domain adaptation for person re-identification," *IEEE Trans. Multimedia*, vol. 23, pp. 1681–1695, 2020.
- [14] M. Long, Y. Cao, J. Wang, and M. Jordan, "Learning transferable features with deep adaptation networks," in *Proc. Int. Conf. Mach. Learn. (ICML)*, Jul. 2015, pp. 97–105.
- [15] M. Long, Z. Cao, J. Wang, and M. Jordan, "Conditional adversarial domain adaptation," in *Proc. Adv. Neural Inform. Process. Syst. (NeurIPS)*, Dec. 2018, pp. 1647–1657.
- [16] M. Long, H. Zhu, J. Wang, and M. Jordan, "Deep transfer learning with joint adaptation networks," in *Proc. Int. Conf. Mach. Learn. (ICML)*, Aug. 2016, pp. 2208–2217.
- [17] J. Hoffman, E. Tzeng, T. Park, J. Zhu, P. Isola, K. Saenko, A. Efros, and T. Darrell, "Cycada: Cycle-consistent adversarial domain adaptation," in *Proc. Int. Conf. Mach. Learn. (ICML)*, Jul. 2018, pp. 1994–2003.
- [18] Y. Zhang, H. Tang, K. Jia, and M. Tan, "Domain-symmetric networks for adversarial domain adaptation," in *Proc. IEEE Conf. Comput. Vis. Pattern Recog. (CVPR)*, Jun. 2019, pp. 5031–5040.
- [19] J. Munro and D. Damen, "Multi-modal domain adaptation for fine-grained action recognition," in *Proc. IEEE Conf. Comput. Vis. Pattern Recog. (CVPR)*, Jun. 2020, pp. 119–129.
- [20] R. Gopalan, R. Li, and R. Chellappa, "Domain adaptation for object recognition: An unsupervised approach," in *Proc. IEEE Int. Conf. Comput. Vis. (ICCV)*, Nov. 2011, pp. 999–1006.
- [21] B. Gong, Y. Shi, F. Sha, and K. Grauman, "Geodesic flow kernel for unsupervised domain adaptation," in *Proc. IEEE Conf. Comput. Vis. Pattern Recog. (CVPR)*, Jun. 2012, pp. 2066–2073.
- [22] R. Caseiro, J.-F. Henriques, P. Martins, and J. Batista, "Beyond the shortest path: Unsupervised domain adaptation by sampling subspaces along the spline flow," in *Proc. IEEE Conf. Comput. Vis. Pattern Recog. (CVPR)*, Jun. 2015, pp. 3846–3854.
- [23] J. Wang, W. Feng, Y. Chen, H. Yu, M. Huang, and P. S. Yu, "Visual domain adaptation with manifold embedded distribution alignment," in *Proc. ACM Int. Conf. Multimedia (ACMMM)*, Oct. 2018, pp. 402–410.
- [24] S. Tang, Y. Ji, J. Lyu, J. Mi, and J. Zhang, "Visual domain adaptation exploiting confidence-samples," in *Proc. IEEE Int. Rob. Syst. (IROS)*, Nov. 2019, pp. 1173–1179.
- [25] S. Tang, M. Ye, P. Xu, and X. Li, "Adaptive pedestrian detection by predicting classifier," *Neural Comput. Appl.*, vol. 31, no. 4, pp. 1189–1200, 2019.
- [26] A. Krause, P. Perona, and R. G. Gomes, "Discriminative clustering by regularized information maximization," in *Proc. Adv. Neural Inform. Process. Syst. (NeurIPS)*, Dec. 2010, pp. 775–783.
- [27] P. Bojanowski and A. Joulin, "Unsupervised learning by predicting noise," in *Proc. Int. Conf. Mach. Learn. (ICML)*, Aug. 2017, pp. 517–526.
- [28] R. Liao, A. Schwing, R. S. Zemel, and R. Urtasun, "Learning deep parsimonious representations," in *Proc. Adv. Neural Inform. Process. Syst. (NeurIPS)*, Dec. 2016, pp. 5083–5091.
- [29] M. Caron, P. Bojanowski, J. Mairal, and A. Joulin, "Unsupervised pre-training of image features on non-curated data," in *Proc. IEEE Int. Conf. Comput. Vis. (ICCV)*, Oct. 2019, pp. 2959–2968.
- [30] J. Xie, R. Girshick, and A. Farhadi, "Unsupervised deep embedding for clustering analysis," in *Proc. Int. Conf. Mach. Learn. (ICML)*, Jun. 2016, pp. 478–487.
- [31] X. Zhan, Z. Liu, J. Yan, D. Lin, and C. C. Loy, "Consensus-driven propagation in massive unlabeled data for face recognition," in *Proc. Springer Eur. Conf. Comput. Vis. (ECCV)*, Sep. 2018, pp. 568–583.
- [32] L. Yang, X. Zhan, D. Chen, J. Yan, C. C. Loy, and D. Lin, "Learning to cluster faces on an affinity graph," in *Proc. IEEE Conf. Comput. Vis. Pattern Recog. (CVPR)*, Jun. 2019, pp. 2298–2306.
- [33] Y. M. Asano, C. Rupprecht, and A. Vedaldi, "Self-labelling via simultaneous clustering and representation learning," in *OpenReview.net Int. Conf. Learn. Represent. (ICLR)*, Apr. 2019.
- [34] W. Chen, S. Pu, D. Xie, S. Yang, Y. Guo, and L. Lin, "Unsupervised image classification for deep representation learning," in *Proc. Springer Eur. Conf. Comput. Vis. (ECCV)*, Aug. 2020, pp. 430–446.
- [35] G. Kang, L. Jiang, Y. Yang, and A. G. Hauptmann, "Contrastive adaptation network for unsupervised domain adaptation," in *Proc. IEEE Conf. Comput. Vis. Pattern Recog. (CVPR)*, Aug. 2019, pp. 4893–4902.
- [36] H. Tang, K. Chen, and K. Jia, "Unsupervised domain adaptation via structurally regularized deep clustering," in *Proc. IEEE Conf. Comput. Vis. Pattern Recog. (CVPR)*, Jun. 2020, pp. 8722–8732.
- [37] F. G. Ashby and W. T. Maddox, "Human category learning," *Annu. Rev. Psychol.*, vol. 56, pp. 149–178, 2005.
- [38] W.-S. Deng and V. M. Sloutsky, "The development of categorization: Effects of classification and inference training on category representation," *Developmental Psychology*, vol. 51, no. 3, pp. 392–405, 2015.
- [39] K. He, X. Zhang, S. Ren, and J. Sun, "Deep residual learning for image recognition," in *Proc. IEEE Conf. Comput. Vis. Pattern Recog. (CVPR)*, Jun. 2016, pp. 1180–1189.
- [40] R. Müller, S. Kornblith, and G. E. Hinton, "When does label smoothing help?" in *Proc. Adv. Neural Inform. Process. Syst. (NeurIPS)*, Dec. 2019, pp. 4696–4705.
- [41] K. Saenko, B. Kulis, M. Fritz, and T. Darrell, "Adapting visual category models to new domains," in *Proc. Springer Eur. Conf. Comput. Vis. (ECCV)*, Sep. 2010, pp. 213–226.
- [42] H. Venkateswara, J. Eusebio, S. Chakraborty, and S. Panchanathan, "Deep hashing network for unsupervised domain adaptation," in *Proc. IEEE Conf. Comput. Vis. Pattern Recog. (CVPR)*, Jul. 2017, pp. 5385–5394.
- [43] X. Peng, B. Usman, N. Kaushik, J. Hoffman, D. Wang, and K. Saenko, "Visda: The visual domain adaptation challenge," *arXiv:1710.06924*, 2017. [Online]. Available: <http://arxiv.org/abs/1710.06924>
- [44] R. Xu, G. Li, J. Yang, and L. Lin, "Larger norm more transferable: An adaptive feature norm approach for unsupervised domain adaptation," in *Proc. IEEE Int. Conf. Comput. Vis. (ICCV)*, Nov. 2019, pp. 1426–1435.
- [45] C. Szegedy, V. Vanhoucke, S. Ioffe, J. Shlens, and Z. Wojna, "Rethinking the inception architecture for computer vision," in *Proc. IEEE Conf. Comput. Vis. Pattern Recog. (CVPR)*, Jun. 2016, pp. 2818–2826.
- [46] Y. Ganin and V. Lempitsky, "Unsupervised domain adaptation by backpropagation," in *Proc. Int. Conf. Mach. Learn. (ICML)*, Jul. 2015.
- [47] Z. Deng, Y. Luo, and J. Zhu, "Cluster alignment with a teacher for unsupervised domain adaptation," in *Proc. IEEE Int. Conf. Comput. Vis. (ICCV)*, Nov. 2019, pp. 9943–9952.
- [48] X. Chen, S. Wang, M. Long, and J. Wang, "Transferability vs. discriminability: Batch spectral penalization for adversarial domain adaptation," in *Proc. Int. Conf. Mach. Learn. (ICML)*, Jun. 2019, pp. 1081–1090.
- [49] C.-Y. Lee, T. Batra, M. H. Baig, and D. Ulbricht, "Sliced wasserstein discrepancy for unsupervised domain adaptation," in *Proc. IEEE Conf. Comput. Vis. Pattern Recog. (CVPR)*, Jul. 2019, pp. 10 285–10 295.
- [50] K. Saito, Y. Ushiku, T. Harada, and K. Saenko, "Adversarial dropout regularization," in *Int. Conf. Learn. Represent. (ICLR)*. OpenReview.net, May. 2018.
- [51] X. Wang, Y. Jin, M. Long, J. Wang, and M. Jordan, "Transferable normalization: Towards improving transferability of deep neural networks," in *Proc. Adv. Neural Inform. Process. Syst. (NeurIPS)*, Nov. 2019, pp. 1951–1961.
- [52] X. Jiang, Q. Lao, S. Matwin, and M. Havaei, "Implicit class-conditioned domain alignment for unsupervised domain adaptation," in *Proc. Int. Conf. Mach. Learn. (ICML)*, vol. 119, Jul. 2020, pp. 4816–4827.
- [53] S. Cui, S. Wang, J. Zhuo, L. Li, Q. Huang, and Q. Tian, "Towards discriminability and diversity: Batch nuclear-norm maximization under label insufficient situations," in *Proc. IEEE Conf. Comput. Vis. Pattern Recog. (CVPR)*, Jun. 2020, pp. 3940–3949.

- [54] G. Yang, H. Xia, M. Ding, and Z. Ding, "Bi-directional generation for unsupervised domain adaptation." in *Proc. Appl. Artif. Intell. conf. (AAAI)*, Feb. 2020, pp. 6615–6622.
- [55] Y. Jin, X. Wang, M. Long, and J. Wang, "Minimum class confusion for versatile domain adaptation," in *Proc. Springer Eur. Conf. Comput. Vis. (ECCV)*, Aug. 2020, pp. 464–480.